
Article:
Lacey, J., Webster, S.J., Heath, P.R. et al. (7 more authors) (2022) Sorting Nexin 24 is required for α-granule biogenesis and cargo delivery in megakaryocytes. Haematologica. ISSN 0390-6078

https://doi.org/10.3324/haematol.2021.279636

---

haematologica
Journal of The Ferrata Storti Foundation

Sorting Nexin 24 is required for α-granule biogenesis and cargo delivery in megakaryocytes

by Joanne Lacey, Simon J. Webster, Paul R. Heath, Chris J. Hill, Lucinda Nicholson-Goult, Bart E. Wagner, Abdullah O. Khan , Neil V. Morgan, Michael Makris and Martina E. Daly

Received: July 14, 2021.
Accepted: January 3, 2022.

Citation: Joanne Lacey, Simon J. Webster, Paul R. Heath, Chris J. Hill, Lucinda Nicholson-Goult, Bart E. Wagner, Abdullah O. Khan , Neil V. Morgan, Michael Makris and Martina E. Daly. Sorting Nexin 24 is required for α-granule biogenesis and cargo delivery in megakaryocytes. Haematologica. 2022 Jan 13. doi: 10.3324/haematol.2021.279636. [Epub ahead of print]

Sorting Nexin 24 is required for α-granule biogenesis and cargo delivery in megakaryocytes

Joanne Lacey,[1] Simon J. Webster,[1] Paul R. Heath,[2] Chris J. Hill,[3] Lucinda Nicholson-Goult,[4] Bart E. Wagner,[4] Abdullah O. Khan,[5] Neil V. Morgan,[5] Michael Makris[1] and Martina E. Daly.[1]

[1]Department of Infection, Immunity and Cardiovascular Disease, University of Sheffield, Sheffield, UK;
[2]Sheffield Institute for Translational Neuroscience (SITraN), Department of Neuroscience, University of Sheffield, Sheffield, UK;
[3]Department of Molecular Biology and Biotechnology, University of Sheffield, Sheffield, UK;
[4]Histopathology Department, Royal Hallamshire Hospital, Sheffield, UK;
[5]Institute of Cardiovascular Sciences, College of Medical and Dental Sciences, University of Birmingham, Birmingham, UK.

Running head: SNX24 and α-granule biogenesis
Corresponding author: Martina E. Daly, E-mail: M.Daly@sheffield.ac.uk
Manuscript: Abstract 246 words; Text 3,974 words; Figures: 5
Appendix: Supplementary methods, 1 table (Table S1), legends to Tables S2 to S9 and figures S1 to S4

Supplementary Excel file: Transcriptome data and results of functional annotation cluster analysis

Acknowledgements

The authors would like to thank the individuals who participated in this study by kindly donating blood samples for transcriptome analysis. This work was supported by the British Heart Foundation through the award of a project grant (PG/15/61/31634). AOK is a Henry Wellcome fellow (218649/Z/19/Z).

Author Contributions

JL and SJW designed and performed the experiments; PRH performed the transcriptome analysis; CJH performed EM on iPSC derived megakaryocytes; LN-G and BEW performed EM on clinical samples; MM recruited the patients; AOK provided guidance on the iPSC differentiation; MED and NVM formulated the research idea and designed the study; MED supervised the study; JL analysed the data, and drafted the first version of the manuscript, which was read and commented on by all authors.

Abstract

Germline defects affecting the DNA-binding domain of the transcription factor FLI1 are associated with a bleeding disorder that is characterised by the presence of large, fused α-granules in platelets. We investigated whether the genes showing abnormal expression in FLI1-deficient platelets could be involved in platelet α-granule biogenesis by undertaking transcriptome analysis of control platelets and platelets harbouring a DNA-binding variant of FLI1. Our analysis identified 2276 transcripts that were differentially expressed in FLI1-deficient platelets. Functional annotation clustering of the coding transcripts revealed significant enrichment for gene annotations relating to protein transport, and identified Sorting nexin 24 (SNX24) as a candidate for further investigation. Using an iPSC-derived megakaryocyte model, *SNX24* expression was found to be increased during the early stages of megakaryocyte differentiation and downregulated during proplatelet formation, indicating tight regulatory control during megakaryopoiesis. CRISPR-Cas9 mediated knockout (KO) of *SNX24* led to decreased expression of immature megakaryocyte markers, CD41 and CD61, and increased expression of the mature megakaryocyte marker CD42b ($p=0.0001$), without affecting megakaryocyte polyploidisation, or proplatelet formation. Electron microscopic analysis revealed an increase in empty membrane-bound organelles in SNX24 KO megakaryocytes, a reduction in α-granules and an absence of immature and mature multivesicular bodies, consistent with a defect in the intermediate stage of α-granule maturation. Co-localisation studies showed that SNX24 associates with each compartment of α-granule maturation. Reduced expression of CD62P and VWF was observed in SNX24 KO megakaryocytes. We conclude that SNX24 is required for α-granule biogenesis and intracellular trafficking of α-granule cargo within megakaryocytes.

Introduction

The ETS transcription factor Friend Leukaemia virus Integration 1, or FLI1, plays a fundamental role in megakaryopoiesis by co-operating with the ETS factor GA binding protein, alpha subunit (GABPA), to regulate the expression of multiple megakaryocyte-specific genes expressed during the early and late stages of megakaryopoiesis.[1,2] Partial deletion of chromosome 11, in a region that includes the gene encoding FLI1 (11q23.3-24), is associated with Paris Trousseau syndrome, which is characterised by dysmegakaryopoiesis in the bone marrow.[3,4] Affected individuals have an increased tendency to bleed, as well as thrombocytopenia characterised by the presence of large platelets containing large fused α-granules in the circulation.[5-7]

Germline defects in FLI1 have also been described.[8-10] Indeed, we previously reported an enrichment of heterozygous *FLI1* defects among patients with excessive bleeding in association with a significant reduction in δ-granule secretion, and mild thrombocytopenia.[8] Further characterisation of two *FLI1* alterations predicting amino acid substitutions in the ETS DNA-binding domain of FLI1 showed that they disrupted transcriptional activity and would therefore cause a reduction in the expression of megakaryocyte-specific genes, providing an explanation for the bleeding tendency observed in the patients.[8] The identification of a homozygous *FLI1* defect, that predicted a substitution in the ETS domain and resulted in a defect in transcription among members of a family affected by a bleeding disorder that resembled Paris Trousseau Syndrome which was characterised by thrombocytopenia and the presence of abnormally large α-granules in a subpopulation of platelets, suggested that the abnormal platelet granules was due to loss of FLI1 activity.[9] The identification of two further *FLI1* defects affecting residues in the ETS domain of FLI1 which were associated with the presence of giant α-granules and depletion of δ-granules support this hypothesis.[10]

While the role of platelet degranulation in maintaining vascular integrity has long been recognised, the pathways leading to the assembly and exocytosis of platelet α- and δ-granules, and the genes that regulate them, remain to be fully established. The biogenesis of α- and δ-granules shares some common features, but the pathways involve distinct protein trafficking machinery.[11,12] Both granules are derived through a process of budding from the *trans*-Golgi network to form vesicles that merge with early endosomes and mature into multivesicular bodies.[13-15] The α-granules can also be derived from the platelet membrane through clathrin-coated pit mediated endocytosis to form vesicles that traffic to the early

endosomes.[15,16] Studies in patients with inherited granule storage disorders[17-19], combined with extensive analyses of platelet lysates, and studies in mice carrying mutations in different secretion genes, have allowed characterisation of the cargo of platelet storage granules, and provided essential information on the secretory machinery of platelets.[20-22]

The abnormally large α-granules and reduced number of δ-granules, and the defect in δ-granule secretion that have been described in platelets from patients harbouring *FLI1* defects likely reflect the disruptions in gene expression that occur either directly or indirectly as a result of the abnormal transcriptional activity of FLI1.[8-10] Furthermore, some of the genes showing disrupted expression in FLI1-deficient platelets displaying granule abnormalities could potentially be involved in platelet granule biogenesis under physiological conditions. We explored this hypothesis by undertaking transcriptome analysis of platelets from subjects harbouring a deleterious defect in *FLI1* (c.1028A>G; p.Tyr343Cys) to identify differentially expressed genes encoding proteins which may be involved in platelet granule biogenesis and secretion, and identified a role for Sorting nexin 24 (SNX24) in platelet granule biogenesis using wild-type and SNX24 knockout (KO) induced pluripotent stem cell (iPSC) derived megakaryocytes to model maturation and platelet production.

Methods

Subjects and platelet transcriptome analysis

Total platelet RNA was isolated from 50 ml peripheral blood samples from two heterozygous carriers of the c.1028A>G transition in *FLI1* and from three sex matched healthy individuals. All subjects were studied in parallel on two separate occasions. The study was approved by the National Research Ethics Service Committee (REC reference: 06/MRE07/36).

Following differential centrifugation to obtain platelet-rich plasma, total platelet RNA was isolated using Trizol (see *Supplementary Methods*). 200 ng of RNA (RIN > 7 as measured on the Agilent Bioanalyser) was converted to double stranded cDNA and transcriptome analysis was carried out using human Clariom D Assay chips (Thermo Fisher), which were washed and stained according to standard manufacturers' protocols. The arrays were scanned using the Affymetrix 3000 7G scanner, and the .CEL files analysed using the Transcriptome Analysis Console (TAC) 4.0 software (Thermo Fisher) to identify genes showing >2 and <-2 fold log change and $p<0.05$.

Functional annotation clustering was carried out for those genes which were differentially expressed using the Database for Annotation, Visualization and Integrated Discovery (DAVID; http://david.abcc.ncifcrf.gov/) with the default settings and a low stringency setting.[23,24]

iPSC differentiation to Megakaryocytes

The Gibco episomal hiPSC line was cultivated feeder-free on Geltrex coated flasks and maintained in StemFlex medium (Thermo Scientific). iPSCs were differentiated to mature megakaryocytes and proplatelets as described previously.[25,26] Details of the cell culture conditions and differentiation of iPSCs are included in the *Supplementary Methods.*

Generation of *SNX24* knockout (KO) cell line

The SNX24 KO cell line was generated using the Alt-R RNP system (Integrated DNA Technologies; IDT). SNX24 crRNA and Atto-555 labelled tracrRNA were annealed and the complex incubated with HiFi Cas9 V3 (IDT) to form stable RNP complexes, which were introduced into iPSCs using Lipofectamine Stem (Life Technologies). For single cell cloning, StemFlex medium was supplemented with CloneR (Stemcell Technologies) and the manufacturers' workflow was followed *(see Supplementary Methods for further details)*.

Gene expression analysis of SNX24 KO iPSCs

Gene expression of lineage specific and cellular markers was measured during SNX24 KO iPSC differentiation by quantitative PCR using an ABI 7900 HT analyser (Applied Biosystems). Further details are included in the *Supplementary Methods*, and all oligonucleotide sequences are listed in *Table S1*.

Characterisation of SNX24 KO iPSC derived megakaryocytes

Differentiation of SNX24 KO cells to proplatelet forming megakaryocytes was assessed by immunofluorescent staining of cells, and imaging using a Zeiss A1 confocal microscope. Further details of the antibodies used, and the methodology are provided in the *Supplementary Methods*.

Transmission electron microscopy (TEM) of platelets and megakaryocytes

FLI1-deficient platelets and iPSC-derived megakaryocytes were examined by TEM using a Philips 400 Transmission EM and a FEI Tecnai TEM respectively. Further details are provided in the *Supplementary Methods.*

Statistical analysis

Results were expressed as means +/- standard deviation. Unless otherwise specified, statistical significance was determined using a Student's t-test with $P<0.05$ considered to be statistically significant. Analyses were performed using GraphPad Prism software.

Results

Transcriptome analysis of FLI1-deficient platelets

Transcriptome analysis was undertaken using the Human Clariom D Assay chips for platelets from a father (P1) and son (P2), both of whom were heterozygous for the c.1028A>G *FLI1* variant predicting a p.Tyr343Cys substitution in the DNA-binding domain of FLI1. Both subjects were recruited to the UK GAPP study with a history of excessive bleeding and a suspected inherited platelet disorder, which was characterised by mild thrombocytopenia and a profound reduction in platelet ATP secretion in response to thrombin. The clinical features, and genotypic and phenotypic characteristics of both subjects have been reported previously.[8] Electron microscopic examination of platelets from both P1 and P2 revealed the presence of giant and fused α-granules similar to those previously described in platelets from subjects with *FLI1* defects (Figure 1A).[9,10] Platelet transcriptomes were also analysed from three healthy male subjects (C1, C2 and C3). Transcripts were considered to be significantly differentially expressed if they had a >2 or <-2 fold log change, and a $P<0.05$. Hierarchical clustering and principal component analysis showed clear differences between the FLI1-deficient platelets from P1 and P2 and normal platelets from C1, C2 and C3 (Figure 1B and Figure S1A). Comparison of gene expression in platelets from the two cases with the c.1028A>G *FLI1* variant with that in normal platelets (C1, C2 and C3) identified 2276 (926 down-regulated and 1350 up-regulated) significantly differentially expressed transcripts in the FLI1-deficient platelets (Figure 1C and Tables S2 and S3 of the supplementary Excel file). The 30 coding transcripts displaying the greatest up- and down-regulation in expression in FLI1-deficient platelets relative to normal platelets are indicated in Figure 1D, while Tables S4 and S5 of the supplementary Excel file lists all coding transcripts showing significant down- and up-regulation in FLI1-deficient platelets.

To identify genes for further investigation, functional annotation clustering of the 1487 differentially expressed coding transcripts was undertaken using the DAVID tool (Table S6 of the supplementary Excel file). This identified 234 clusters, which were enriched for multiple

classes of annotation categories. Given our interest in platelet granule biogenesis and secretion, we focused on the GO terms associated within the top four clusters: protein transport, cell-cell adhesion, endoplasmic reticulum, and late endosome (Figure 1E and Table S7 of the supplementary Excel file). Together these clusters included three of the 30 most differentially expressed genes; *SNX24*, *HBE1* and *TESPA1*. Of these, *SNX24* was the most downregulated, having a 45.91 fold reduction in expression in FLI1-deficient platelets compared with normal platelets (FDR P-value = 0.0034), and was the only one of the nine genes represented in a subgroup of 53 genes from the cluster that were enriched for the GO term 'protein transport' (P = 0.024) (Figure 1E and F and Table S8 of the supplementary Excel file). The 232 genes associated with GO terms in the top four annotation clusters are listed by their gene symbols and descriptions, and expression levels in Table S9 (Supplementary Excel file). Further work focused on *SNX24*. qPCR of *SXN24* expression using independent probes confirmed its down-regulation in platelet RNA isolated from both P1 and P2 (Figure S1B).

SNX24 is required during early megakaryopoiesis

SNX24 is a member of the sorting nexin family of proteins which are defined by the presence of a Phox homology (PX) phosphoinositide-binding domain and play essential roles in regulating protein trafficking, through all stages of the endocytic pathway. While a specific role for SNX24 in platelets has not been demonstrated, variants of *SNX24* have been associated with platelet crit and mean platelet volume[27,28], and more recently, *SNX24* was shown to be upregulated in megakaryocytes with ploidy.[29] These findings, and our observation that *SNX24* was downregulated in FLI1-deficient platelets displaying abnormal α-granules, suggest a role for SNX24 in platelet formation which we explored further in iPSC derived proplatelet forming megakaryocytes.

We generated an SNX24 KO in iPSCs using CRISPR guides targeting the first exon of *SNX24* and confirmed the absence of *SNX24* expression in two clones by qPCR (Figure S2A). Further analysis confirmed that both clones were homozygous KO, and that both the wild-type and KO cells retained normal karyotypes (Figure S2B-E). We used established procedures to differentiate iPSCs (OCT4+) to hematopoietic progenitors derived from haemogenic endothelium (CD34+; day 0-6), then to immature megakaryocytes (CD41+/CD42-; day 6-12) before terminal differentiation to mature proplatelet forming megakaryocytes (CD41+/CD42+; day 12-17) (Figure 2A). qPCR to assess expression of specific markers of stem cells (OCT4), hematopoietic stem cells (CD34) and megakaryocytes (CD61/GpIIIa, CD41/GPIIb and CD42b/GPIbα) confirmed the expected

expression for the different stages of differentiation of the wild-type iPSCs (Figure S3A). Similarly, assessment of *FLI1* expression by qPCR showed the expected increase in expression during MK maturation as FLI1 regulates the expression of both early and late MK-specific genes (Figure S3B).[2] Examination of *SNX24* expression during differentiation of wild-type iPSCs showed that it steadily increased during the early stages of megakaryocyte differentiation and was subsequently downregulated during proplatelet formation (Figure 2B). This suggests that expression of *SNX24* is tightly controlled during megakaryopoiesis.

We observed a decrease in expression of the immature megakaryocyte markers (CD41 and CD61) and an increase in expression of the mature megakaryocyte marker (CD42b) at Day 12 of differentiation of the SNX24 KO iPSCs, suggesting the presence of more mature megakaryocyte progenitors (Figure 2C and D, and Figure S3C). SNX24 KO iPSCs generated megakaryocytes with similar ploidy numbers to the wild-type iPSCs, suggesting depletion of SNX24 does not inhibit polyploidization (Figure 2E). SNX24 KO cells also retained the ability to generate proplatelet forming megakaryocytes after terminal differentiation (Figure 2F). These data suggest a potential role for SNX24 in the early stages of megakaryopoiesis during megakaryocyte progenitor formation.

SNX24 depletion causes loss of granule content

To assess whether SNX24 plays a role in granule formation, we examined the ultrastructure of SNX24 KO megakaryocytes by transmission electron microscopy (TEM). We observed several organelles in wild-type iPSC derived megakaryocytes including α-granules, δ-granules, endosomal intermediates (MVBI and MVBII) and mitochondria. We defined an α-granule as a single membrane enclosing a matrix and a δ-granule as a round organelle with a high-density core surrounded by a white rim. There was a dramatic increase in the presence of empty membrane bound organelles in the SNX24 KO cells, though the mitochondria appeared unaffected (Figure 3A). The empty spherical organelles, multivesicular subclasses and tubular shaped compartments were suggestive of morphologically distinct stages of α-granules. δ-granules could not be accurately evaluated in iPSC derived megakaryocytes, where unstained EM would be more informative. Wild-type megakaryocytes contained early endosomal compartments packed with vesicles and intraluminal contents, multivesicular bodies (MVBs) with intraluminal vesicles and late endosomes with intraluminal contents. Loss of SNX24 resulted in empty intermediate endosomal compartments during granule biogenesis (Figure 3B). These findings support the participation of SNX24 in the biogenesis and maturation of MVBs as well as in the development of α-granules.

SNX24 localises to α-granules and endosomal compartments

We explored whether SNX24 is required for the biogenesis of α-granules and endosomal precursors using confocal fluorescence microscopy to examine its co-localisation with markers for α-granules (CD62P), early endosomes (EEA1), late endosomes and MVBs (Rab7a) in megakaryocytes. We observed SNX24 localisation in iPSC derived megakaryocytes, which we identified by multiple nuclei (N). In megakaryocytes, SNX24 partially co-localised with CD62P in punctate structures in 2N and 6N megakaryocytes (Figure 4A). We observed that SNX24 was localised to both larger α-granules and smaller punctate structures, which we speculate could be transport vesicles. SNX24 was also associated with the plasma membrane where it was distributed as small puncta and aggregated clusters, some of which co-localised with CD62P. SNX24 expression was low in the proplatelets but still co-localised to CD62P positive punctate structures (Figure 4B).

SNX24 was partially co-localised with early endosomes in megakaryocytes around the plasma membrane, and associated with EEA1 positive compartments (Figure 4C). SNX24 also associates with Rab7a positive late endosomes and MVBs (Figure 4D). These observations indicate that SNX24 is associated with each stage of α-granule maturation, and suggest that it may traffic from early endosomes to mature α-granules.

We also examined gene expression of markers specific for early endosomes (Rab5a) and MVBs (Rab7a) in SNX24 KO megakaryocytes. Interestingly, Rab5a and Rab7a gene expression was significantly increased in SNX24 KO megakaryocytes compared to the wild-type cells, which was consistent with disruption to the endosomal trafficking pathway (Figure S4). In contrast, NBEAL2 expression was significantly decreased in the SNX24 KO megakaryocytes, supporting the involvement of SNX24 at an earlier stage of α-granule development than NBEAL2 (Figure S4).

SNX24 KO cells lack α-granule cargo

The appearance of empty α-granules and intermediate endosomal compartments in SNX24 KO cells is suggestive of a depletion in α-granule cargo. Furthermore, the distribution pattern of SNX24 around the cell periphery and in α-granule compartments suggests it may be involved in the trafficking of α-granule cargo. We therefore examined the subcellular distribution of α-granule cargo (CD62P, VWF) in SNX24 KO megakaryocytes. We observed

a reduction in CD62P and VWF staining in megakaryocytes, indicating an α-granule trafficking defect (Figure 5A and B). RT-qPCR analysis confirmed that CD62P and VWF gene expression was significantly reduced in SNX24 KO cells (Figure 5C and D). These findings indicate a requirement for SNX24 for trafficking of both soluble (VWF) and membrane (CD62P) cargo.

Discussion

The pathways leading to platelet granule biogenesis and exocytosis, and the genes that regulate them, remain to be fully established. In this study, we sought to identify candidate genes that potentially contribute to platelet granule biogenesis by taking advantage of the changes in gene expression that occur in platelets from individuals with germline mutations that affect the transcriptional activity of FLI1, which also display abnormal α-granules. Thus, transcriptome analysis of platelets harbouring a DNA-binding variant of FLI1 revealed significant differences in expression profiles of FLI1-deficient and wild-type platelets with 2276 transcripts identified as being differentially expressed in the FLI1-deficient platelets. Functional annotation clustering of the differentially expressed coding transcripts revealed significant enrichment for annotations relating to protein transport, and led us to focus on SNX24, a protein not previously implicated in platelet granule biogenesis. We confirmed that *SNX24* was significantly downregulated in expression in the FLI1-deficient platelets and observed that SNX24 is localised throughout the α-granule biogenesis pathway, associating with early endosomes, multivesicular bodies and α-granules. Furthermore, loss of *SNX24* disrupts the endosomal trafficking pathway in megakaryocytes, resulting in an α-granule defect and decreased expression of α-granule proteins. Our findings lead us to propose that SNX24 is a novel component of the protein sorting machinery during α-granule maturation.

The sorting nexins (SNXs) are a diverse family of cytoplasmic and membrane-associated proteins that are involved in endocytosis, endosomal sorting and endosomal signalling. They are characterized by the presence of a conserved phox-homology (PX) domain which binds specific phosphoinositides, facilitating targeting of proteins to distinct endosomal compartments.[30] Sorting nexins play critical roles in many aspects of cellular function, and dysfunction of SNX proteins has been described in association with a variety of human disorders including neurodegenerative diseases, pathologic infection, cancer and cardiovascular disease.[31,32] SNX24 is one of a subgroup of the SNX protein family that is relatively poorly characterised, though GWAS have associated variants of SNX24 with platelet crit and volume.[27,28] An interesting correlation between the *SNX24* single nucleotide polymorphism (rs28891) and complications due to coronary artery aneurysm in Kawasaki

disease has also been reported, and in the same study siRNA knockdown of SNX24 was shown to significantly decrease expression of the proinflammatory cytokines IL-1 beta, IL-6, and IL-8 in lipopolysaccharide-treated human umbilical vein endothelial cells.[33] Interestingly, α-granules contain a wide range of chemokines including IL-8.[21] Other sorting nexins have been implicated in platelet granule formation. In particular, SNX17 was identified in a yeast two-hybrid screen as an interaction partner of P-selectin[34] and it is thought that SNX17 may regulate the endocytosis of P-selectin from the plasma membrane and inhibit trafficking to lysosomes.[35]

The mechanism underlying the significant downregulation of *SNX24* in FLI1-deficient platelets is unclear. Previous work which mapped the genome-wide FLI1-binding sites in primary human megakaryocytes indicates that FLI1 does not bind directly to the *SNX24* promoter.[36] The reduced expression is more likely to be an indirect effect of FLI1 loss, potentially through GABPA which acts in concert with FLI1 to regulate megakaryocyte gene expression, since GABPA gene expression was significantly upregulated in the FLI1-deficient platelets and it is predicted to bind to the SNX24 promoter.[37]

We used functional annotation clustering as a tool to prioritise candidate genes encoding proteins that may be involved in platelet granule biogenesis, focusing our attention on the cluster which was enriched for the GO annotation of 'protein transport' which included SNX24. Interestingly, this subgroup also included SEC22B, Homolog B Vesicle Trafficking Protein, a membrane resident trafficking protein which was recently shown to be required for α-granule biogenesis in megakaryocytes which was upregulated in the FLI1-deficient platelets.[38] Though further work would be required to determine if any of the remaining genes in this subgroup are required for platelet granule formation, this observation nonetheless supports the use of transcriptome analysis from FLI1-deficient platelets as an approach to identify novel components of the granule biogenesis machinery.

We used iPSC derived megakaryocytes to study the role of SNX24 during megakaryopoiesis, comparing wild-type cells and SNX24 KO cells which were generated using CRISPR-Cas9 gene editing. *SNX24* expression appears to be tightly regulated during megakaryopoiesis, being highest during early megakaryopoiesis at the megakaryocyte progenitor stage, and dropping significantly in mature proplatelet-forming megakaryocytes. We observed that SNX24 KO cells have a higher proportion of mature CD42b+ megakaryocyte progenitors. However, loss of SNX24 did not inhibit formation of polyploid megakaryocytes or proplatelet forming megakaryocytes. In contrast to wild-type megakaryocytes, TEM analysis of SNX24 KO megakaryocytes showed a reduction in α-

granules and an increase in the presence of empty vacuoles, resembling the phenotype seen in platelets from patients with Gray Platelet Syndrome, which is characterised by the presence of empty α-granules.[39] SNX24 KO cells were also devoid of immature type I MVBs that contain internal vesicles, and type II MVBs that contain internal vesicles and an electron dense core. The ultrastructural abnormalities observed in SNX24 KO megakaryocytes are consistent with defects in the intermediate stages of α-granule maturation and resemble those seen in VPS33B KO cells.[40]

Studies in patients with inherited defects that cause deficiencies in α-granule cargo and number have yielded valuable insights into the mechanisms underlying platelet granule biogenesis. Thus, defects in the genes encoding the VPS33B-VPS16B complex, and the BEACH-domain containing NBEAL2, have been shown to underlie the absence of α-granules in arthrogryposis, renal dysfunction and cholestasis (ARC) syndrome and in Grey Platelet syndrome respectively.[19,41,42,18,43] Loss of VPS33B results in the absence of α-granules, decreased levels of α-granule cargo and a reduction in MVBs.[40,44] Likewise, loss of VPS16B results in reduced or undetectable α-granule proteins as well as a complete absence of α-granules from platelets.[41] The VPS33B/16B complex localises on endosomes and promotes protein trafficking between MVBs and α-granules.[45] Megakaryocytes deficient in NBEAL2 show a loss of α-granules and a reduction in α-granule cargo proteins such as VWF but retain some CD62P[46] and Sec22b was recently identified as an interaction partner of NBEAL2, that facilitates α-granule cargo stability and granule development.[38]

Our TEM observations denote an α-granule defect in SNX24 KO cells, leading us to assess if SNX24 was distributed within α-granules and intermediate compartments. We have shown that SNX24 is co-localised with CD62P in α-granules during megakaryopoiesis. Vesicles carrying α-granule cargo bud off from either the trans-Golgi network or plasma membrane and are subsequently directed to MVBs via endosomes.[13] We show that SNX24 is co-localised with the early endosome marker EEA1 around the cell periphery, and partially associated with Rab7+ multivesicular bodies. This suggests that SNX24 traffics between, or binds to α-granule components during their maturation. Likewise, known α-granule machinery such as VPS16B and VPS33B traffic between late endosomes and α-granules.[42] We observed that loss of SNX24 leads to a reduction in expression of α-granule cargo including VWF and CD62P. P-selectin is a membrane protein that contains a signal peptide to direct it towards the developing granule.[47] VWF is a soluble protein that self-assembles into large aggregates and eventually forms tubular structures within α-granules.[48] The differences in expression of VWF and CD62P seen in SNX24 KO cells could reflect differential packaging or vesicle transport to distinct subcompartments within α-granules.

Further studies will be required to define the role of SNX24 in intracellular trafficking. In particular, it will be important to investigate its expression throughout megakaryopoiesis and to determine, more precisely, the point at which loss of SNX24 disrupts the trafficking of α-granule cargo and leads to the appearance of empty vacuoles, though our findings suggest it occurs early during maturation as 2N megakaryocytes derived from SNX24 KO cells lack α-granule cargo. Given its downregulation in mature proplatelet-forming megakaryocytes, and that loss of *SNX24* did not inhibit formation of polyploid megakaryocytes or proplatelet forming megakaryocytes, it would be interesting to know the role of SNX24, if any, in platelets. There are no disorders reported to be associated with the SNX24 gene, and there are no phenotyping or viability data available for the Snx24 knockout mouse[49], but it would be interesting to assess the appearance and behaviour of their platelets, and to compare them with platelets derived from SNX24 KO megakaryocytes.

In conclusion, we have presented data that evidence a requirement for SNX24 in α-granule biogenesis and the intracellular trafficking of α-granule cargo within megakaryocytes. Future studies characterising the molecular interactions of SNX24 will likely reveal further insights into the underlying molecular machinery and protein complexes required for α-granule formation in platelets.

References

1. Li Y, Luo H, Liu T, Zacksenhaus E, Ben-David Y. The *ets* transcription factor Fli-1 in development, cancer and disease. Oncogene. 2014;34(16):2022-2031.
2. Pang L, Xue H-H, Szalai G, et al. Maturation stage-specific regulation of megakaryopoiesis by pointed-domain Ets proteins. Blood. 2006;108(7):2198-2206.
3. Hromas R, May W, Denny C, et al. Human FLI-1 localizes to chromosome 11Q24 and has an aberrant transcript in neuroepithelioma. Biochim Biophys Acta. 1993;1172(1-2):155-158.
4. Breton-Gorius J, Favier R, Guichard J, et al. A new congenital dysmegakaryopoietic thrombocytopenia (Paris-Trousseau) associated with giant platelet alpha-granules and chromosome 11 deletion at 11q23. Blood. 1995;85(7):1805-1814.
5. Hart A, Melet F, Grossfeld P, et al. Fli-1 is required for murine vascular and megakaryocytic development and is hemizygously deleted in patients with thrombocytopenia. Immunity. 2000;13(2):167-177.

6. Favier R, Jondeau K, Boutard P, et al. Paris-Trousseau syndrome : clinical, hematological, molecular data of ten new cases. Thromb Haemost. 2003;90(5):893-897.
7. Raslova H, Komura E, Le Couédic JP, et al. FLI1 monoallelic expression combined with its hemizygous loss underlies Paris-Trousseau/Jacobsen thrombopenia. J Clin Invest. 2004;114(1):77-84.
8. Stockley J, Morgan NV, Bem D, et al. Enrichment of FLI1 and RUNX1 mutations in families with excessive bleeding and platelet dense granule secretion defects. Blood. 2013;122(25):4090-4093.
9. Stevenson WS, Rabbolini DJ, Beutler L, et al. Paris-Trousseau thrombocytopenia is phenocopied by the autosomal recessive inheritance of a DNA-binding domain mutation in FLI1. Blood. 2015;126(17):2027-2030.
10. Saultier P, Vidal L, Canault M, et al. Macrothrombocytopenia and dense granule deficiency associated with FLI1 variants: ultrastructural and pathogenic features. Haematologica. 2017;102(6):1006-1016.
11. Machlus KR, Italiano JE Jr. The incredible journey: From megakaryocyte development to platelet formation. J Cell Biol. 2013;201(6):785-796.
12. Sharda A, Flaumenhaft R. The life cycle of platelet granules. F1000Res. 2018;7:236.
13. Heijnen HF, Debili N, Vainchencker W, Breton-Gorius J, Geuze HJ, Sixma JJ. Multivesicular bodies are an intermediate stage in the formation of platelet alpha-granules. Blood. 1998;91(7):2313-2325.
14. Ambrosio AL, Boyle JA, Di Pietro SM. Mechanism of platelet dense granule biogenesis: study of cargo transport and function of Rab32 and Rab38 in a model system. Blood. 2012;120(19):4072-4081.
15. Chen Y, Yuan Y, Li W. Sorting machineries: how platelet-dense granules differ from α-granules. Biosci Rep. 2018;38(5):BSR20180458.
16. Behnke O. Coated pits and vesicles transfer plasma components to platelet granules. Thromb Haemost. 1989;62(2):718-722.
17. Wei AH, Li W. Hermansky-Pudlak syndrome: pigmentary and non-pigmentary defects and their pathogenesis. Pigment Cell Melanoma Res. 2013;26(2):176-192.
18. Gunay-Aygun M, Falik-Zaccai TC, Vilboux T, et al. NBEAL2 is mutated in gray platelet syndrome and is required for biogenesis of platelet α-granules. Nat Genet. 2011;43(8):732-734.
19. Gissen P, Johnson CA, Morgan NV, et al. Mutations in VPS33B, encoding a regulator of SNARE-dependent membrane fusion, cause arthrogryposis-renal dysfunction-cholestasis (ARC) syndrome. Nat Genet. 2004;36(4):400-404.

20. Kahr WH, Lo RW, Li L, et al. Abnormal megakaryocyte development and platelet function in Nbeal2(-/-) mice. Blood. 2013;122(19):3349-3358.
21. Blair P, Flaumenhaft R. Platelet alpha-granules: basic biology and clinical correlates. Blood Rev. 2009;23(4):177-189.
22. Nurden P, Stritt S, Favier R, Nurden AT. Inherited platelet diseases with normal platelet count: phenotypes, genotypes and diagnostic strategy. Haematologica. 2021;106(2):337-350.
23. Huang DW, Sherman BT, Lempicki RA. Systematic and integrative analysis of large gene lists using DAVID Bioinformatics Resources. Nature Protoc. 2009;4(1):44-57.
24. Huang DW, Sherman BT, Lempicki RA. Bioinformatics enrichment tools: paths toward the comprehensive functional analysis of large gene lists. Nucleic Acids Res. 2009;37(1):1-13.
25. Feng Q, Shabrani N, Thon JN, et al. Scalable generation of universal platelets from human induced pluripotent stem cells. Stem Cell Reports. 2014;3(5):817-831.
26. Khan AO, Slater A, Maclachlan A, et al. Post-translational polymodification of β1-tubulin regulates motor protein localisation in platelet production and function. Haematologica. 2020 Dec 17. [Epub ahead of print]
27. Astle WJ, Elding H, Jiang T, et al. The Allelic Landscape of Human Blood Cell Trait Variation and Links to Common Complex Disease. Cell. 2016;167(5):1415-1429.
28. Vuckovic D, Bao EL, Akbari P, et al. The Polygenic and Monogenic Basis of Blood Traits and Diseases. Cell. 2020;182(5):1214-1231.
29. Choudry FA, Bagger FO, Macaulay IC, et al. Transcriptional characterization of human megakaryocyte polyploidization and lineage commitment. J Thromb Haemost. 2021;19(5):1236-1249.
30. Haft CR, de la Luz Sierra M, Barr VA, Haft DH, Taylor SI. Identification of a family of sorting nexin molecules and characterization of their association with receptors. Mol Cell Biol. 1998;18(12):7278-7287.
31. Hanley SE, Cooper KF. Sorting Nexins in Protein Homeostasis. Cells. 2020;10(1):17.
32. Yang J, Villar VAM, Rozyyev S, Jose PA, Zeng C. The emerging role of sorting nexins in cardiovascular diseases. Clin Sci (Lond). 2019;133(5):723-737.
33. Lin YJ, Chang JS, Liu X, et al. Sorting nexin 24 genetic variation associates with coronary artery aneurysm severity in Kawasaki disease patients. Cell Biosci. 2013;3(1):44.
34. Florian V, Schlüter T, Bohnensack R. A new member of the sorting nexin family interacts with the C-terminus of P-selectin. Biochem Biophys Res Commun. 2001;281(4):1045-1050.

35. Williams R, Schlüter T, Roberts MS, Knauth P, Bohnensack R, Cutler DF. Sorting nexin 17 accelerates internalization yet retards degradation of P-selectin. Mol Biol Cell. 2004;15(7):3095-3105.
36. Tijssen MR, Cvejic A, Joshi A, et al. Genome-wide analysis of simultaneous GATA1/2, RUNX1, FLI1, and SCL binding in megakaryocytes identifies hematopoietic regulators. Dev Cell. 2011;20(5):597-609.
37. Fishilevich S, Nudel R, Rappaport N, et al. GeneHancer:genome-wide integration of enhancers and target genes in GeneCards. Database (Oxford). 2017;2017:bax028.
38. Lo RW, Li L, Pluthero FG, Leung R, Eto K, Kahr WHA. The endoplasmic reticulum protein SEC22B interacts with NBEAL2 and is required for megakaryocyte α-granule biogenesis. Blood. 2020;136(6):715-725.
39. Maynard DM, Heijnen HF, Gahl WA, Gunay-Aygun M. The α-granule proteome: novel proteins in normal and ghost granules in gray platelet syndrome. J Thromb Haemost. 2010;8(8):1786-1796.
40. Bem D, Smith H, Banushi B, et al. VPS33B regulates protein sorting into and maturation of α-granule progenitor organelles in mouse megakaryocytes. Blood. 2015;126(2):133-143.
41. Urban D, Li L, Christensen H, et al. The VPS33B-binding protein VPS16B is required in megakaryocyte and platelet α-granule biogenesis. Blood. 2012;120(25):5032-5040.
42. Kahr WH, Hinckley J, Li L, et al. Mutations in NBEAL2, encoding a BEACH protein, cause gray platelet syndrome. Nat Genet. 2011;43(8):738-740.
43. Albers CA, Cvejic A, Favier R, et al. Exome sequencing identifies NBEAL2 as the causative gene for gray platelet syndrome. Nat Genet. 2011;43(8):735-737.
44. Lo B, Li L, Gissen P, Christensen H, et al. Requirement of VPS33B, a member of the Sec1/Munc18 protein family, in megakaryocyte and platelet alpha-granule biogenesis. Blood. 2005;106(13):4159-4166.
45. Ambrosio AL, Di Pietro SM. Mechanism of platelet α-granule biogenesis: study of cargo transport and the VPS33B-VPS16B complex in a model system. Blood Adv. 2019;3(17):2617-2626.
46. Lo RW, Li L, Leung R, Pluthero FG, Kahr WHA. NBEAL2 (NeurobeachinLike 2) Is Required for Retention of Cargo Proteins by α-Granules During Their Production by Megakaryocytes. Arterioscler Thromb Vasc Biol. 2018;38(10):2435-2447.
47. Disdier M, Morrissey JH, Fugate RD, Bainton DF, McEver RP. Cytoplasmic domain of P-selectin (CD62) contains the signal for sorting into the regulated secretory pathway. Mol Biol Cell. 1992;3(3):309-321.

48. Huang RH, Wang Y, Roth R, et al. Assembly of Weibel-Palade body-like tubules from N-terminal domains of von Willebrand factor. Proc Natl Acad Sci U S A. 2008;105(2):482-487.

49. Dickinson, M, Flenniken A, Ji X et al. High-throughput discovery of novel developmental phenotypes. Nature. 2016;537(7621):508-514.

Figure Legends

Figure 1: Transcriptome analysis of FLI1-deficient platelets identifies *SNX24* for further investigation

A. Representative electron micrographs of platelets from P1 and P2, displaying large and fused a-granules (indicated by yellow arrows).

B. Hierarchical clustering of differentially expressed transcripts in control (C1, C2, C3) and FLI1-deficient (P1, P2) platelets. All samples were analysed in parallel on two occasions.

C. Volcano plot showing the transcripts which are downregulated (green) or upregulated (red) in FLI1-deficient platelets relative to control platelets.

D. Log fold change of the 30 most downregulated and upregulated coding transcripts observed in FLI1-deficient platelets relative to control platelets (<2 or ≥2 fold change, FDR ≤ 0.05).

E. Functional annotation clustering of differentially expressed coding transcripts using DAVID identified 234 annotation clusters. GO terms from the top 4 annotation clusters which were significantly enriched are shown and the Log10 p-value for each GO term is displayed on the X-axis. The numbers of upregulated and downregulated genes with each GO term are indicated.

F. Log fold change of the 15 most downregulated (green) and upregulated (red) genes showing enrichment for the GO terms protein transport, cell adhesion, endoplasmic reticulum and late endosome (<2 or ≥2 fold change, FDR ≤ 0.05).

Figure 2: Characterisation of SNX24 KO iPSC derived Megakaryocytes

A. Schematic of iPSC differentiation to megakaryocytes.

B. qPCR analysis of *SNX24* expression during iPSC differentiation to megakaryocytes. n=3 experiments. P<0.0001 = ****and p<0.01 = **, Student's t-test.

C. Immunofluorescence staining for CD41 (green) and CD42 (red) in wild-type cells at day 12 of differentiation. Nuclei are counterstained with Hoechst 33342. Scale bar 50µm.

D. qPCR analysis of CD41, CD61 and CD42 gene expression in Day 12 wild-type and SNX24 KO megakaryocyte progenitors. P<0.0001 = **** and P<0.001 = ***, Student's t-test, n=2

E. Representative confocal microscopy fluorescence images of CD41 (green) and CD42 (red) in wild-type and SNX24 KO megakaryocytes. Nuclei are counterstained with Hoechst 33342. Scale bar 20µm.

F. Brightfield images of proplatelets in wild-type and SNX24 KO cells. Scale bar 20µm.

Figure 3: SNX24 KO megakaryocytes lack α-granules

A. Representative transmission electron micrographs of wild-type (WT) and SNX24 KO megakaryocytes. Spherical and tubular α-granules (arrow heads) are observed in wild-type cells and absent in SNX24 KO cells. The upper panels are low magnification with a scale bar of 2µm. The lower panels are high magnification images with a scale bar of 0.5µm.

B. Electron micrographs of wild-type cells and SNX24 KO cells. MVBs (arrow heads) containing intraluminal vesicles were observed in wild-type cells but not in SNX24 KO cells. The upper panels are low magnification images with a scale bar of 1µm. The lower panels are high magnification images with a scale bar of 0.5µm.

Figure 4: SNX24 localises to α-granules and endosomal intermediates.

A. Representative confocal microscopy images of wild-type early megakaryocytes (upper panel) and late megakaryocytes (lower panel) stained with anti-SNX24 (green) and anti-CD62 (red). Nuclei are counterstained with Hoechst 33342. Scale bar 20µm.

B. Representative confocal microscopy images of wild-type proplatelets stained with anti-SNX24 (green) and anti-CD62 (red). Nuclei are stained with Hoechst 33342. Scale bar 20µm

C. Representative confocal microscopy images of wild-type megakaryocytes stained with anti-SNX24 (green) and anti-EEA1(red). Nuclei are stained with Hoechst 33342. Scale bar 10µm.

D. Representative confocal fluorescence microscopy images of wild-type megakaryocytes immunostained with anti-SNX24 (green) and anti-Rab7a(red). Nuclei are stained with Hoechst 33342. Scale bar 10µm.

Figure 5: Abnormal trafficking of α-granule proteins in SNX24 KO cells

A. Representative confocal microscopy images of wild-type and SNX24 KO megakaryocytes immunostained with anti-VWF (green) and anti-CD42 (red). Nuclei are stained with Hoechst 33342. Scale bar 20µm.

B. Representative confocal microscopy images of wild-type and SNX24 KO megakaryocytes immunostained with anti-CD62P (green) and anti-CD42 (red). Nuclei are stained with Hoechst 33342. Scale bar 20µm.

C. qPCR analysis of VWF gene expression in Day12 wild-type and SNX24 KO megakaryocytes. $p<0.0001$ = ****, Student's t-test, n=2.

D. qPCR analysis of CD62P gene expression in Day12 wild-type and SNX24 KO megakaryocytes. $p<0.01$ = **, Student's t-test, n=2.

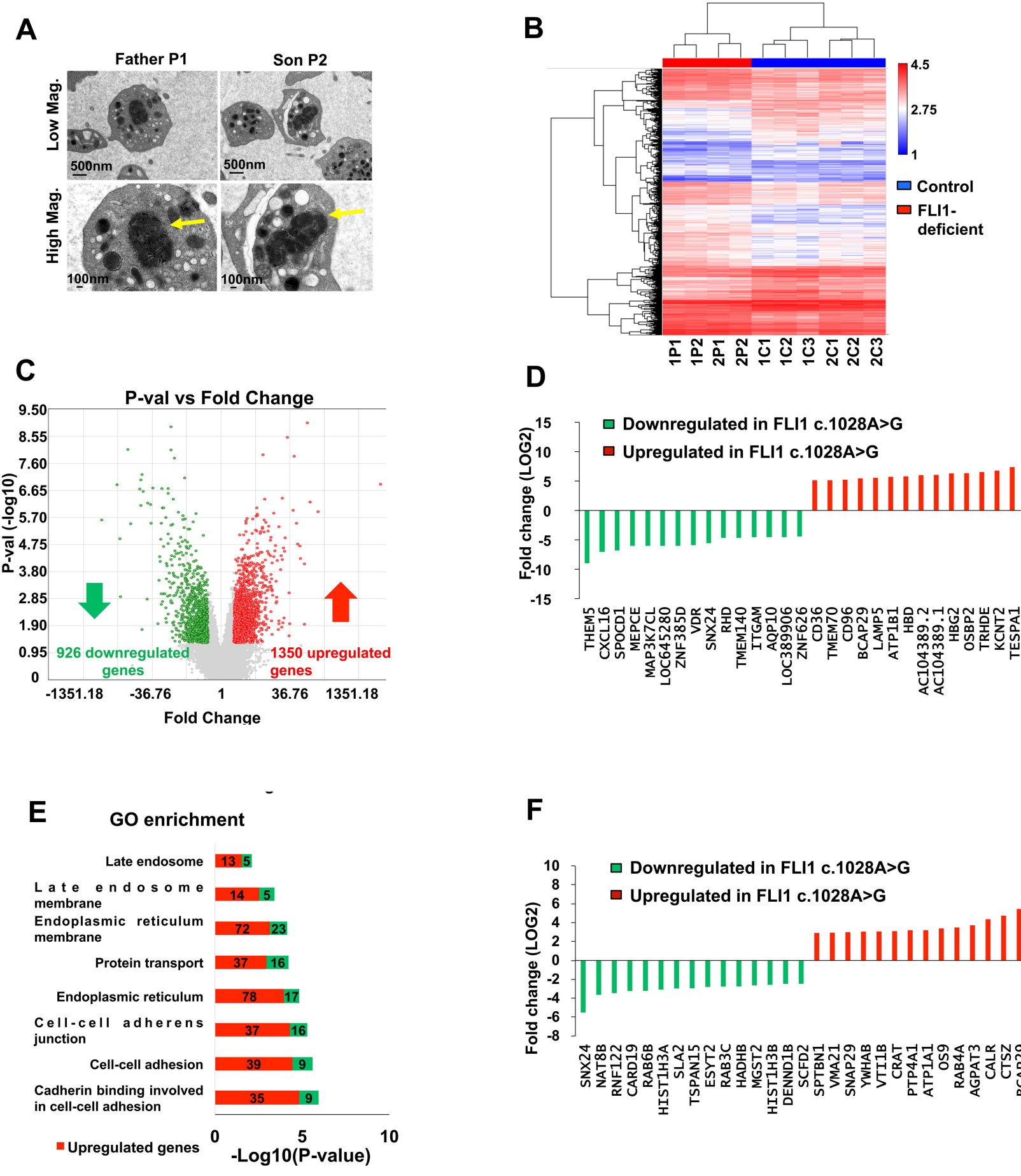
A
Father P1
Son P2
Low Mag.
High Mag.
500nm
500nm
100nm
100nm
B
4.5
2.75
1
Control
FLI1-deficient
1P1
1P2
2P1
2P2
1C1
1C2
1C3
2C1
2C2
2C3
C
P-val vs Fold Change
P-val (-log10)
9.50
8.55
7.60
6.65
5.70
4.75
3.80
2.85
1.90
0.95
0
926 downregulated genes
1350 upregulated genes
-1351.18
-36.76
1
36.76
1351.18
Fold Change
D
Downregulated in FLI1 c.1028A>G
Upregulated in FLI1 c.1028A>G
Fold change (LOG2)
15
10
5
0
-5
-10
-15
THEM5
CXCL16
SPOCD1
MEPCE
MAP3K7CL
LOC645280
ZNF385D
VDR
SNX24
RHD
TMEM140
ITGAM
AQP10
LOC389906
ZNF626
CD36
TMEM70
CD96
BCAP29
LAMP5
ATP1B1
HBD
AC104389.2
AC104389.1
HBG2
OSBP2
TRHDE
KCNT2
TESPA1
HBE1
E
GO enrichment
Late endosome
13
5
Late endosome membrane
14
5
Endoplasmic reticulum membrane
72
23
Protein transport
37
16
Endoplasmic reticulum
78
17
Cell-cell adherens junction
37
16
Cell-cell adhesion
39
9
Cadherin binding involved in cell-cell adhesion
35
9
Upregulated genes
0
5
10
-Log10(P-value)
F
Downregulated in FLI1 c.1028A>G
Upregulated in FLI1 c.1028A>G
Fold change (LOG2)
10
8
6
4
2
0
-2
-4
-6
-8
SNX24
NAT8B
RNF122
CARD19
RAB6B
HIST1H3A
SLA2
TSPAN15
ESYT2
RAB3C
HADHB
MGST2
HIST1H3B
DENND1B
SCFD2
SPTBN1
VMA21
SNAP29
YWHAB
VTI1B
CRAT
PTP4A1
ATP1A1
OS9
RAB4A
AGPAT3
CALR
CTSZ
BCAP29
TESPA1

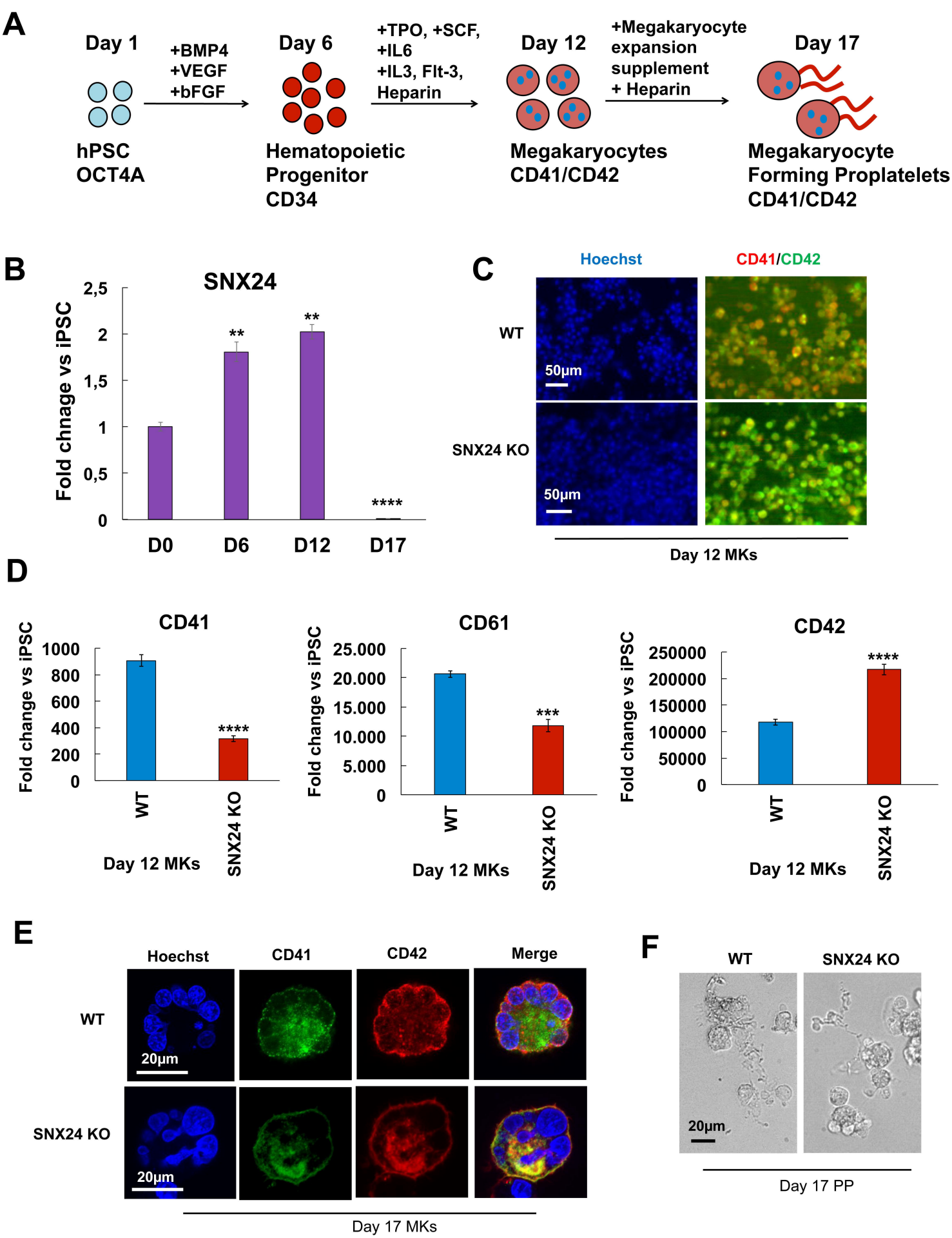
A
Day 1
+BMP4
+VEGF
+bFGF
Day 6
+TPO, +SCF,
+IL6
+IL3, Flt-3,
Heparin
Day 12
+Megakaryocyte
expansion
supplement
+ Heparin
Day 17
hPSC
OCT4A
Hematopoietic
Progenitor
CD34
Megakaryocytes
CD41/CD42
Megakaryocyte
Forming Proplatelets
CD41/CD42
B
SNX24
Fold chnage vs iPSC
2,5
2
1,5
1
0,5
0
**
**
****
D0
D6
D12
D17
C
Hoechst
CD41/CD42
WT
SNX24 KO
50µm
50µm
Day 12 MKs
D
CD41
Fold change vs iPSC
1000
800
600
400
200
0
****
WT
SNX24 KO
Day 12 MKs
CD61
Fold change vs iPSC
25.000
20.000
15.000
10.000
5.000
0
***
WT
SNX24 KO
Day 12 MKs
CD42
Fold change vs iPSC
250000
200000
150000
100000
50000
0
****
WT
SNX24 KO
Day 12 MKs
E
Hoechst
CD41
CD42
Merge
WT
SNX24 KO
20µm
20µm
Day 17 MKs
F
WT
SNX24 KO
20µm
Day 17 PP

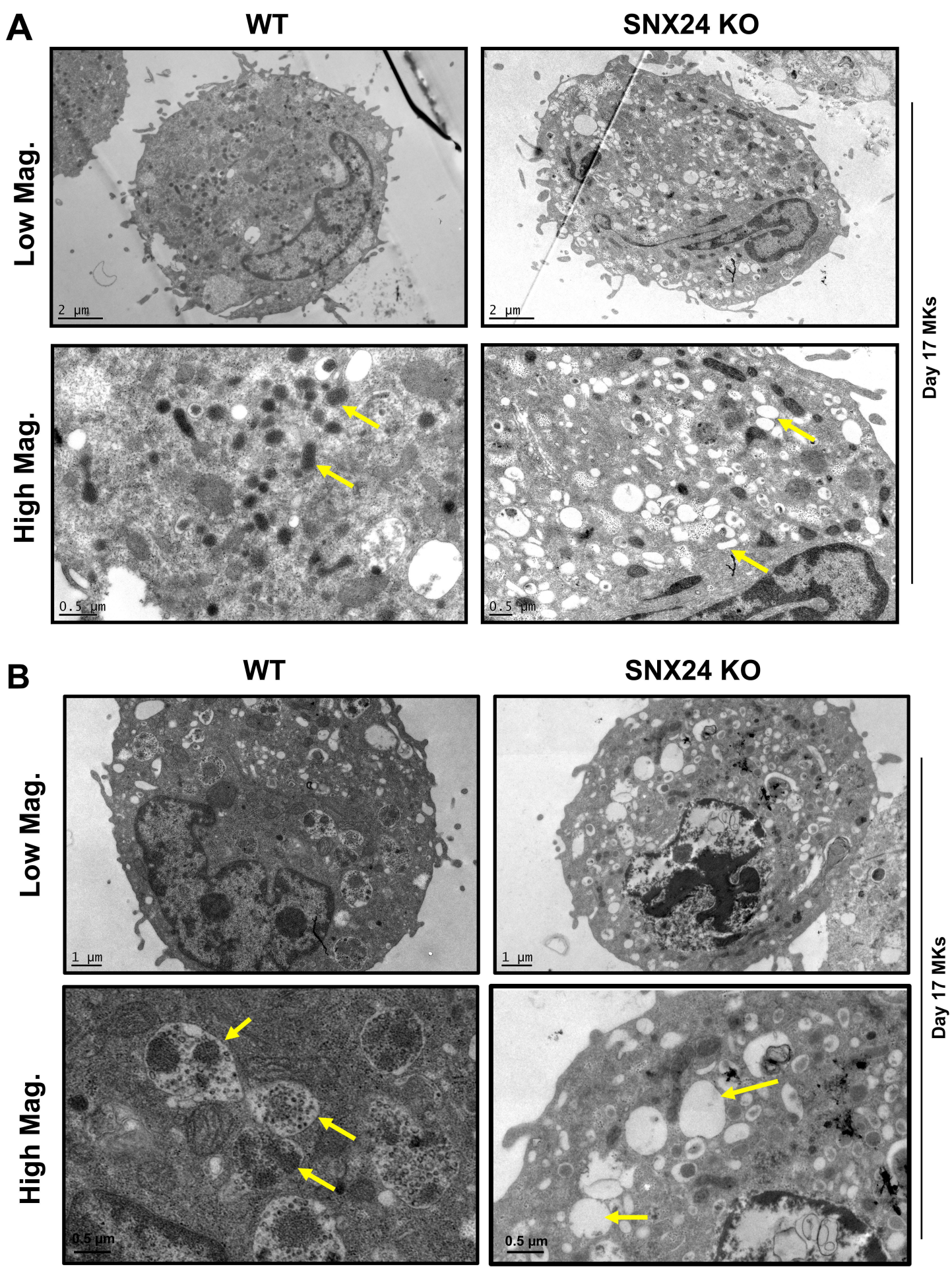
A
WT
SNX24 KO
Low Mag.
High Mag.
2 µm
2 µm
0.5 µm
0.5 µm
Day 17 MKs
B
WT
SNX24 KO
Low Mag.
High Mag.
1 µm
1 µm
0.5 µm
0.5 µm
Day 17 MKs

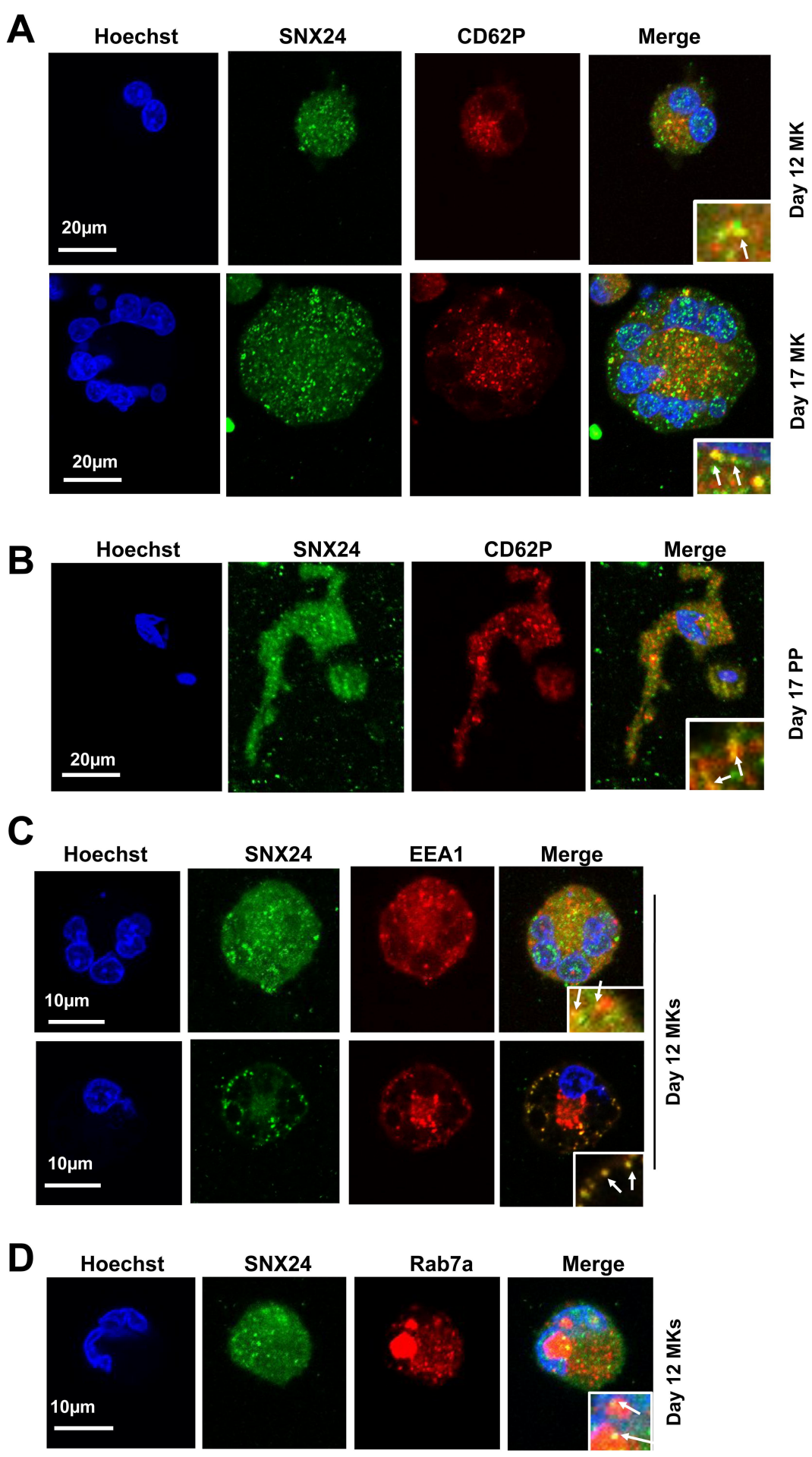
A
Hoechst
SNX24
CD62P
Merge
20μm
Day 12 MK
20μm
Day 17 MK
B
Hoechst
SNX24
CD62P
Merge
20μm
Day 17 PP
C
Hoechst
SNX24
EEA1
Merge
10μm
10μm
Day 12 MKs
D
Hoechst
SNX24
Rab7a
Merge
10μm
Day 12 MKs

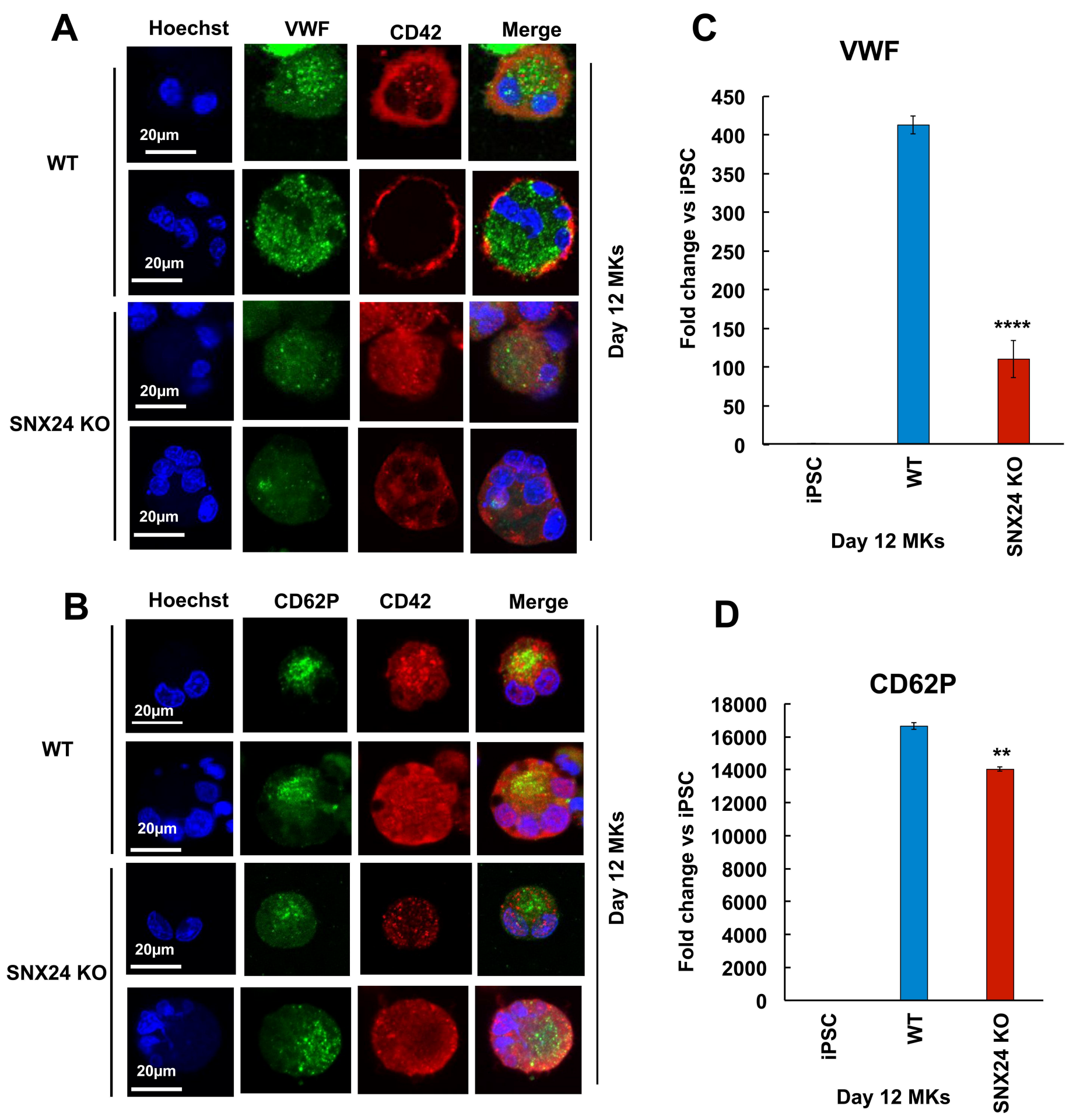
A
Hoechst
VWF
CD42
Merge
WT
SNX24 KO
20μm
Day 12 MKs
B
Hoechst
CD62P
CD42
Merge
WT
SNX24 KO
20μm
Day 12 MKs
C
VWF
Fold change vs iPSC
450
400
350
300
250
200
150
100
50
0
****
iPSC
WT
SNX24 KO
Day 12 MKs
D
CD62P
Fold change vs iPSC
18000
16000
14000
12000
10000
8000
6000
4000
2000
0
**
iPSC
WT
SNX24 KO
Day 12 MKs

Sorting Nexin 24 is required for α-granule biogenesis and cargo delivery in megakaryocytes

Joanne Lacey,[1] Simon J. Webster,[1] Paul R. Heath,[2] Chris J. Hill,[3] Lucinda Nicholson-Goult,[4] Bart E. Wagner,[4] Abdullah O. Khan,[5] Neil V. Morgan,[5] Michael Makris[1] and Martina E. Daly.[1]

[1]Department of Infection, Immunity and Cardiovascular Disease, University of Sheffield, Sheffield, UK;
[2]Sheffield Institute for Translational Neuroscience (SITraN), Department of Neuroscience, University of Sheffield, Sheffield, UK;
[3]Department of Molecular Biology and Biotechnology, University of Sheffield, Sheffield, UK;
[4]Histopathology Department, Royal Hallamshire Hospital, Sheffield, UK;
[5]Institute of Cardiovascular Sciences, College of Medical and Dental Sciences, University of Birmingham, Birmingham, UK.

Supplementary Methods

Preparation of platelet RNA

Platelet RNA was prepared as described previously.[1] Briefly, peripheral blood samples were centrifuged (200g, 20 min) before carefully removing the platelet rich plasma (PRP). Red blood cells and leukocytes were removed by an additional centrifugation (200g, 10 min) step. The supernatant was collected and platelets harvested by centrifugation (800g, 10 min). Platelet pellets were dissolved in 1mL TRIzol (Thermo Scientific) per 100mg of platelets. Platelet RNA was isolated using TRIzol and then further purified using an RNeasy MinElute Cleanup Kit (Qiagen).

Human pluripotent stem cell culture

The Gibco episomal hiPSC line was purchased from Thermo Scientific and cultivated feeder-free in Geltrex coated flasks. Briefly, Geltrex was diluted 1:100 in DMEM F12 and incubated at 37°C for 1h prior to plating cells. hiPSCs were maintained in StemFlex medium (Thermo Scientific). Routine clump passaging was performed every 4-5 days using 0.5mM EDTA following manufacturer's instructions (Sigma). TrypLE was used for single cell seeding during transfection or single cell cloning following manufacturer's instructions (Thermo Scientific).

iPSC differentiation to megakaryocytes

Mature megakaryocytes and proplatelet forming megakaryocytes were derived from hiPSCs.[2,3] Briefly, iPSCs were clump passaged onto Collagen Type IV (Advanced Biomatrix) coated dishes (5µg/cm^2) in Stemflex medium containing RevitaCell (Life Technologies). For phase one of the differentiation (Day 1-6), APELII medium (Stem Cell Technologies) was supplemented with 50ng/mL BMP-4 (ThermoScientific), 50ng/mL FGF-β (Stem Cell Technologies) and 50ng/mL VEGF (Stem Cell Technologies). For phase two of the differentiation (Day 6-12), cells were incubated in APELII containing 25ng/mL TPO (Stem Cell Technologies), 25ng/mL SCF (Stem Cell Technologies), 25ng/mL Flt-3 (Stem Cell Technologies), 10ng/mL Interleukin-3 (Stem Cell Technologies), 10 ng/mL Interleukin-6 (Stem Cell Technologies) and 5U/mL Heparin (Stem Cell Technologies). During Day 6-12, cells were collected by centrifugation at 400 g for 5 min and frozen in 10% FBS/DMSO. For terminal differentiation, all frozen cells were thawed and plated onto low attachment dishes (Corning) containing StemSpanII (Stem Cell Technologies) supplemented with Megakaryocyte Expansion supplement (Stem Cell Technologies) and 5U/mL Heparin.

CRISPR-Cas9 mediated generation of SNX24 KO cell line

The SNX24 KO cell line was generated using the Alt-R RNP system (IDT). SNX24 crRNA (2nmol) was resuspended in 1x TE pH7.4 at a concentration of 100µM. Atto-555 labelled tracrRNAs (5nmol) were resuspended in 1x TE pH7.4 at a concentration of 100µM. 4.4µL of crRNA and 4.4µL of tracrRNA were added to 1.2 µL of Nuclease Free Duplex Buffer. The mixture was incubated at 95°C for 5 min before cooling at -1°C/sec to 25°C. 1µL of crRNA/tracrRNA mix was then added to 0.6 µL of HiFi Cas9 V3 (IDT; Cat # 1081058) at a ratio of 42pmol:37pmol. The samples were incubated for 20 min at room temperature to form stable RNP complexes. Lipofectamine Stem (Life Technologies) was used to transfect RNP complexes into iPSCs, following the manufacturer's instructions for Stemflex conditions.

Single cell cloning

For single cell cloning, Stemflex medium was supplemented with CloneR (Stemcell Technologies) and the manufacturer's instructions were followed. Briefly, 96-well plates were coated with geltrex and the single cell suspension harvested using TrypLE (Thermo Scientific). Cells were sorted on a BD FACSMelody Cell Sorter directly into 96-well plates. Immediately after sorting, the plates were centrifuged at 1000 rpm for 1 min to aid attachment of the cells. Colonies were allowed to develop for 10-14 days before passaging those wells containing iPSC colonies.

Analysis of genome editing in CRISPR generated clones

Genomic DNA was isolated after single cell cloning using QuickExtract DNA Extraction Solution (Lucigen). Oligonucleotide primers were designed to amplify the CRISPR targeted region of *SNX24* and incorporated EcoRI and SalI sites to facilitate cloning. The Alt-R Genome Editing Detection kit (IDT) was used according to the manufacturer's instructions to screen all single cell clones for *SNX24* editing. PCR products with mismatches indicating editing were cloned between the EcoRI and SalI sites of YCplac33 and plasmid DNA was isolated using the QIAprep Spin Miniprep Kit (Qiagen). Plasmid DNA was sequenced to obtain sequences for both alleles (Source Bioscience).

Qualitative Real Time PCR (qPCR)

RNA was extracted using the RNA Purification Plus kit (Geneflow) and reverse-transcribed into cDNA using the High-Capacity cDNA Reverse Transcription kit (Applied Biosystems). PCRs were set up in triplicate, with each 10µl sample containing 1X TaqMan Fast Universal Master Mix (ThermoFisher), 100nM of the forward and reverse primers (Supplementary

Table 1), 100nM of the appropriate probe from the Universal Probe Library (Roche) and 10ng of cDNA (Applied Biosystems). Each UPL probe is indicated in the supplementary primer table. Using an ABI 7900 HT analyser (Applied Biosystems) samples were heated to 50°C for 2 min and denatured at 95°C for 10 min, before being subjected to 40 cycles of 95°C for 15s and 60°C for 1 min. The Ct values obtained were analysed using the delta-delta Ct method and normalised using either *GAPDH* or *ACTB* as housekeeping genes.

Immunofluorescence

Cells were fixed in a solution of 3.7% paraformaldehyde for 15 min at room temperature, and then permeabilised with 0.2% Triton-X in PBS for 15 min at room temperature. Non-specific binding was blocked by incubation for 1 hour in 1% bovine serum albumin (BSA). Cells were then incubated with primary antibodies at a dilution of 1:200, in PBS supplemented with 1% BSA and 0.1% Tween20, either for 1h at room temperature or overnight at 4°C. The following primary antibodies were used in this study: CD62P (Fisher Scientific), CD42/GPIb (Universal Biologicals), CD41 (Thermo Fisher), VWF (Thermo Fisher), Rab5a (CellSignalling), EEA1 (CellSignalling), Rab7a (CellSignalling), SNX24 (Thermo Fisher). Following three washes with PBS, cells were incubated with fluorescent-dye conjugated secondary antibodies diluted 1:200 in PBS supplemented with 1% BSA and 0.1% Tween20. The following secondary antibodies were used in this study: anti-Mouse Alexa fluor 488, anti-Mouse Alexa fluor 568, anti-Rabbit Alexa fluor 488, anti-Rabbit Alexa fluor 594 (Invitrogen). Nuclei were stained by incubating cells with 10µg/ml Hoechst 33342 for 1 hour at room temperature before washing three times with PBS and imaging. Cells that were prepared for confocal imaging were grown on glass coverslips and mounted onto slides with one drop of Vectashield Mounting Medium (Vector Laboratories).

Fluorescence Microscopy

Images were acquired using a Zeiss A1 confocal microscope with a 63x oil immersion lens, and a Hammamatsu camera. LED power and exposure time were the same within each experiment across different samples. Using NIS-Elements software, five images were taken per sample as representative Z-stacks, and presented as a maximum intensity projection. ND2 files containing z-stacks were processed using FIJI ImageJ software. Equal numbers of 0.15µm slices were used to compare wild-type and SNX24 KO cells.

Electron microscopy of platelets

Platelets were fixed and embedded into TAAB EMIX medium grade epoxy resin and 85nm sections stained in saturated uranyl acetate in 99% ethanol, and Reynold's lead citrate. Sections were viewed on a Philips 400 transmission electron microscope.

Electron microscopy of megakaryocytes

Megakaryocytes were fixed in 2.5% Glutaraldehyde/0.1M Sodium Cacodylate buffer, postfixed in 2% aqueous Osmium Tetroxide, dehydrated through a graded series of ethanol, cleared in epoxypropane (EPP) and then infiltrated in a 50:50 mixture of Araldite resin and EPP overnight with rotation. This mixture was replaced twice over 8 hours with fresh Araldite resin mixture before being embedded and cured in a 60°C oven for 48-72 hours. Ultrathin sections, approximately 85nm thick, were cut using a Leica UC6 ultramicrotome onto 200 mesh copper grids, stained with saturated aqueous Uranyl Acetate followed by Reynold's Lead Citrate and examined using an FEI Tecnai Transmission Electron Microscope at an accelerating voltage of 80Kv. Electron micrographs were recorded using a Gatan Orius 1000B digital camera and Gatan Digital Micrograph software.

Karyotyping

Karyotyping by G-banding was performed by the Sheffield Diagnostic Genetics Service (https://www.sheffieldchildrens.nhs.uk/sdgs/). Cells were treated with 0.1µg/ml KaryoMAX Colcemid Solution in PBS (Life Technologies) for 2 - 4h to arrest cells in metaphase. Cells were harvested and resuspended in 0.0375M KCl. Cells were incubated for 10 min in KCl, collected by centrifugation and fixed with methanol:acetic acid. Metaphase cells were prepared on glass microscope slides and stained with 4:1 Gurr's/Leishmann's stain (Sigma-Aldrich). Banded metaphases were imaged on the Leica Biosystems Cytovision Image Analysis system. At least 20 metaphases were analysed.

References

1. Amisten S. A rapid and efficient platelet purification protocol for platelet gene expression studies. Methods Mol Biol. 2012;788:155-72.
2. Feng Q, Shabrani N, Thon JN, et al. Scalable generation of universal platelets from human induced pluripotent stem cells. Stem Cell Reports. 2014;3(5):817-31.
3. Khan AO, Slater A, Maclachlan A, et al. Post-translational polymodification of β1-tubulin regulates motor protein localisation in platelet production and function. Haematologica. 2020;Online ahead of print. doi: 10.3324/haematol.2020.270793. PMID: 33327716.

Supplementary Tables.

Table S1: Primer and probe sequences.

Name	UPL probe number	Sequence
SNX24 crRNA		tctcttcatagcgaaaggac
SNX24 F cloning		atatatgaattcagcccgcagacctgagtc
SNX24 R cloning		atatatgtcgacctgaactaattgtacagaacttg
SNX24 F	1	cgtcctttcgctatgaagaga
SNX24 R	1	ttcttccattcattagcacttctatc
OCT4 F	78	gtggagagcaactccgatg
OCT4 R	78	tgcagagctttgatgtcctg
CD34 F	78	gtgaaattgactcagggcatc
CD34 R	78	cccctgtccttcttaaactcc
CD41a F	60	gagacacccatgtgcagga
CD41a R	60	agctggggcacacatacg
CD42b F	68	ccttcggaggtctttctgc
CD42b R	68	atggggtgggggtgtaag
SELP F	78	acctgccatttctcttgtgac
SELP R	78	cccctggagtaggaagtgatg
GAPDH F	60	agccacatcgctcagacac
GAPDH R	60	gcccaatacgaccaaatcc
CD61 F	19	ccatcatgcaggctacagtc
CD61 R	19	aaacaccagcaagtgggatg
VWF F	68	ttccaggactgcaacaagc
VWF R	68	agcaatggtgtcgcagaag
ACTB F	38	tcgtgcgtgacattaaggag
ACTB R	38	caggcagctcgtagctcttc

EEA1 F	2	gctgaagaatcagtcagaaagtca
EEA1 R	2	ccttctgctcttgtacctggtc
NBEAL2 F	1	tgctaccactggatgagctg
NBEAL2 R	1	aggttcctgcagagaatgatg
Rab5a F	38	ccaaccaggaatcagtgttgt
Rab5a R	38	actgggctggttaaatgctc
Rab7a F	18	gacaggctagtcacaatgcaga
Rab7a R	18	gtagaaggccacaccgagag
FLI1 F	1	agatccagctgtggcaattc
FLI1 R	1	gtgatacagctggcgttgg

Tables S2 to S9: Transcriptome data and annotation cluster analysis

The transcriptome data and results of annotation cluster analysis are provided as a series of tables in a separate excel file. The first sheet in the excel file provides a key to the eight tables, which correspond to sheets 2 to 9 of the file as shown below.

Table S2: Expression of transcripts showing significant upregulation in FLI1-deficient platelets.

Table S3: Expression of transcripts showing significant downregulation in FLI1-deficient platelets.

Table S4: Expression of coding transcripts showing significant downregulation in FLI1-deficient platelets.

Table S5: Expression of coding transcripts showing significant upregulation in FLI1-deficient platelets.

Table S6: Differentially expressed coding transcripts identified by Ensembl name.

Table S7: Results of DAVID analysis showing the four annotation clusters having the highest enrichment scores.

Table S8: Genes associated with GO terms in the four annotation clusters having the highest enrichment scores.

Table S9: Names, descriptions and expression levels of genes associated with GO terms in the four annotation clusters having the highest enrichment scores.

Supplementary Figures

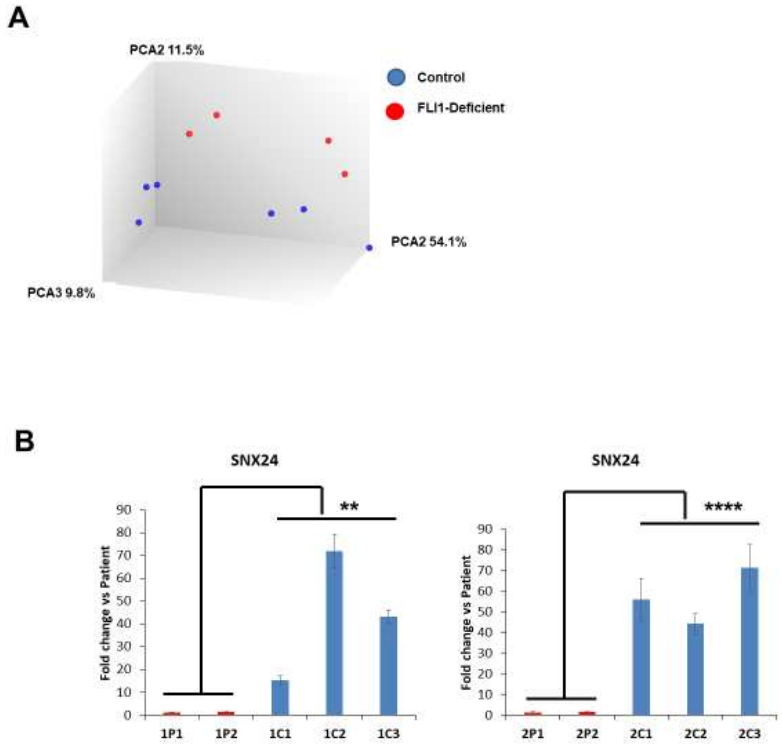

Figure S1: Transcriptome analysis of FLI1-deficient platelets

A. Principal component analysis of FLI1-deficient (red) and control (blue) samples used for microarray analysis.

B. RT-qPCR analysis of *SNX24* expression using independent primers in control and FLI1-deficient platelets. n=3 experiments. Samples were analysed in parallel on two occasions. P<0.0001 = **** and p<0.01 = **, Student's t-test.

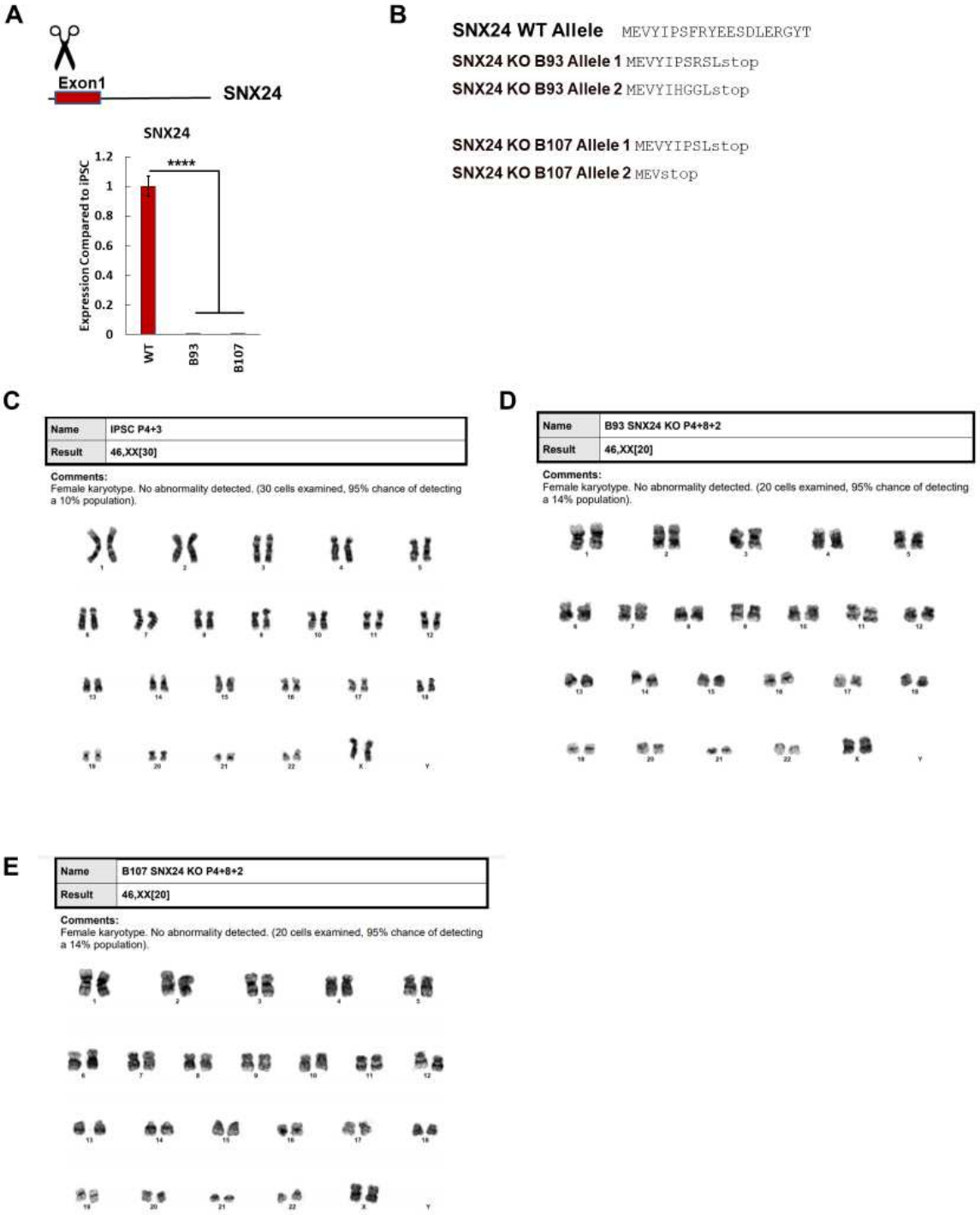

Figure S2: Generation of SNX24 KO cell line

A. CRISPR gene editing of *SNX24* in iPSCs and qPCR analysis of *SXN24* expression in wild-type (WT) and SNX24 KO clones. n=3 experiments. P<0.0001 = ****, Student's t-test
B. Multiple sequence alignment of SNX24 KO clones showing amino acid sequence predicted by both alleles.
C. Karyotype report for wild-type iPSC cells showing a normal karyotype.
D. Karyotype report for SNX24 KO clone B93 showing a normal karyotype.
E. Karyotype report for SNX24 KO clone B107 showing a normal karyotype.

Supplementary Figure S3

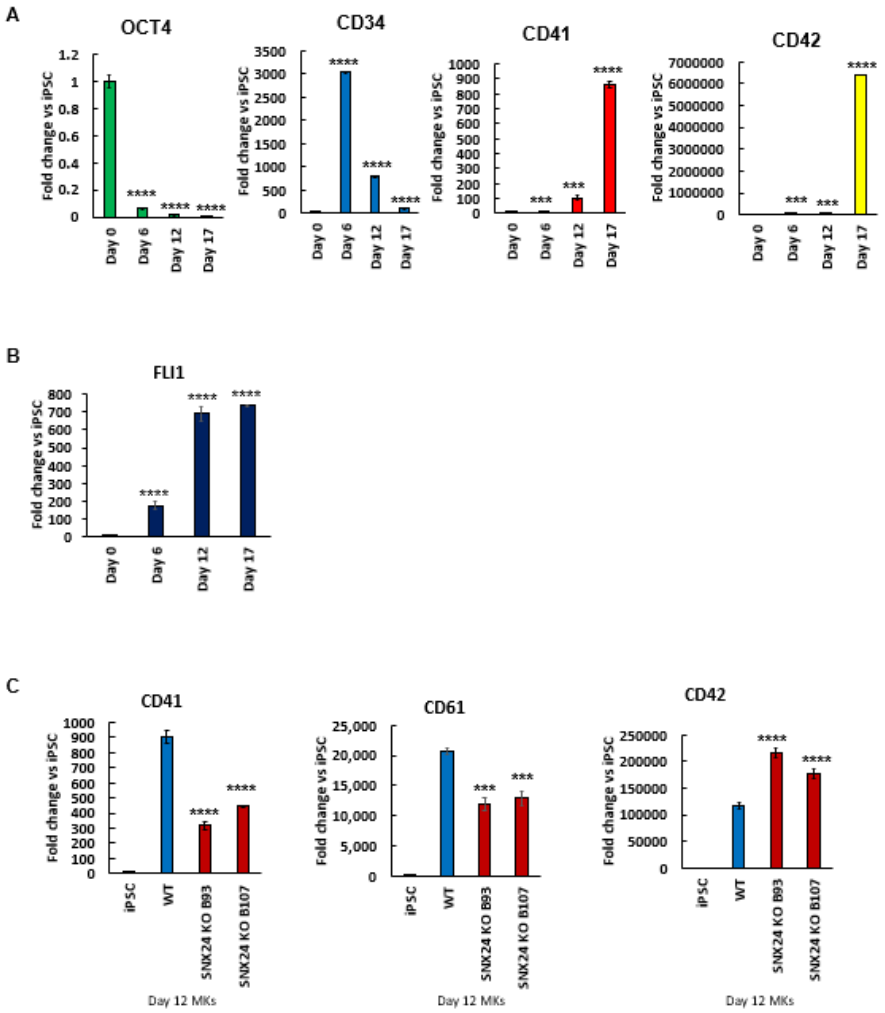

Figure S3: Characterisation of SNX24 KO Megakaryocytes

A. qPCR gene expression analysis of OCT4, CD34, CD41 and CD42 from Day0-Day17 of iPSC differentiation. P<0.0001 = **** and P<0.001 = ***, Student's t test, n=3.
B. qPCR analysis of *FLI1* expression during iPSC differentiation to megakaryocytes. P<0.0001 = ****, Student's t test, n=2.
C. qPCR gene expression analysis of CD41, CD61 and CD42 in WT and SNX24 KO clones (B93 and B107) on Day12 of differentiation P<0.0001 **** and P<0.001 = ***, Student's t test, n=2.

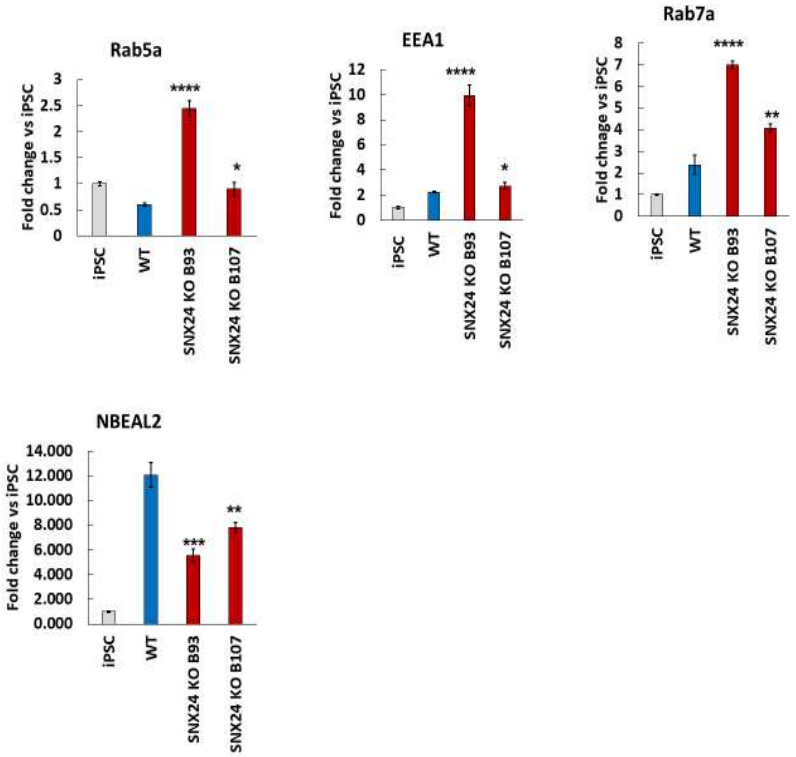

Figure S4: Disruption to endosomal intermediates in SNX24 KO cells

qPCR analysis of EEA1, Rab5a, Rab7a and NBEAL2 expression in Day12 wild-type (WT) and SNX24 KO megakaryocytes. $p<0.0001$ = ****, $p<0.001$ = ***, $p<0.01$ = **, $p<0.05$ = *, Student's t test, n=2